





Charging Mobile Devices in Indoor Environments

Diogo Matos ^{1,†} , Ricardo Pereira ^{1,†} , Helena Ribeiro ^{1,†} , Bernardo Mendes ^{1,†} , Daniel Belo ^{2,†} , Arnaldo Oliveira ^{1,†}  and Nuno Borges Carvalho ^{1,†} 

¹ Instituto de Telecomunicações, Departamento de Eletrónica Telecomunicações e Informática, Univeridade de Aveiro, 3810-193 Aveiro, Portugal; (diogo.silva.matos; r.pereira; helenalsribeiro; bernardomendes; arnaldo.oliveira; nbcarvalho)@ua.pt

² Huawei Technologies Sweden AB, 16494 Kista, Sweden; daniel.belo@huawei.com

* Correspondence: nbcarvalho@ua.pt;

† These authors contributed equally to this work.

Abstract: Wireless power transfer promises to revolutionize the way we use and power mobile devices. However, low transfer efficiencies prevent this technology from seeing wide scale real-world adoption. The aim of this work is to use quasi-optics to develop a system composed of a dielectric lens fed by a phased array to reduce spillover losses, increasing the beam efficiency, while working on the antenna system's Fresnel zone. The DC-RF electronics, digital beamforming and beam-steering by an FPGA, and radiating 4x4 microstrip patch phased array have been developed and experimented upon, while the lens has been designed and simulated. This paper details these preliminary results, where the phased array radiation pattern was measured, showing that the beam is being generated and steered as expected, prompting the lens construction for the complete system experimentation.

Keywords: wireless power transfer; microwaves; DC-RF conversion; beamforming; beamsteering; phased array; microstrip patch; dielectric lens; antenna characterization

1. Introduction

Wireless power transfer (WPT) has been researched since the experiments of Heinrich Hertz [1] and Nikola Tesla [2,3] in the 19th century. Since then, two main technology areas can be identified: coupling and radiative WPT.

The first of which includes the near-field electromagnetic (EM) effects, such as capacitive and inductive coupling, which are useful for a very limited range. A review of near-field WPT can be found in [4]. These have been developed significantly, having reached the point of commercial implementation, with most household electronics having the possibility of being wirelessly charged, such as mobile phones.

The main limitation of near-field WPT is its limited range, as most applications work only up to a few centimeters. Therefore, the transmitting and receiving devices must be very close together and usually have to be properly aligned, restricting the components' movement. Important implementations of near-field WPT can be found nonetheless, such as in biomedical applications [5].

On the other hand, radiative WPT consists in using antennas for radiating EM energy that will propagate through space. In order to achieve high beam efficiency, the radiation should be focused and directed towards a receiving device. This WPT category has also seen intense research, ever since the work of William Brown [1,6]. He proved the viability of these systems by focusing microwave beams into targets, developing high efficiency WPT experiments that still hold records today. Following his work, several nations became interested in radiative WPT, with multiple projects starting all over the world [7-9].

Although long range systems have been proposed, radiative WPT still has to be developed before being widely implemented in real-life scenarios. This is mainly due to low overall efficiencies. One of the most problematic areas is the beam efficiency, mainly due to spillover losses and low coupling to radiating elements. To do that, this work is based on the quasi-optical (QO) theory [10], which studies EM radiation by comparing it to gaussian beams, taking into account the beam divergence. The authors have experience

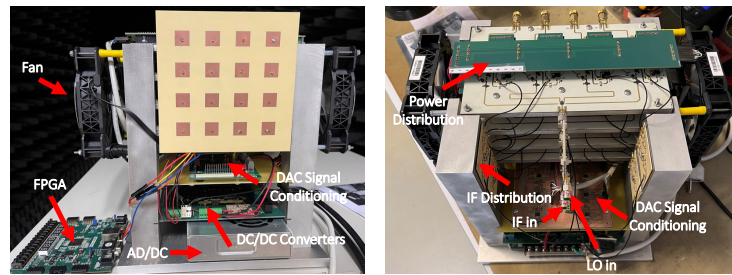


Figure 1. System overview.

with this theory as previous work has been developed on using reflectors for focusing beams in WPT systems [11,12].

Therefore, this work aims to study a more compact and feasible system by transferring power in an indoor environment for charging mobile devices, such as phones, by using quasi-optics for increasing the beam efficiency. To achieve this goal, a beam launcher and a dielectric lens for focusing the beam must be developed.

The first of which is a 4x4 microstrip patch phased-array antenna. By controlling each elements' current distribution, beamforming [13] and beamsteering [14] can be implemented. This is fed by a transmitter that follows a heterodyne architecture, that allow an independent control of each element and can provide a maximum of 2W per element.

Following the gaussian beam generation, it will be focused by a dielectric lens [10], whose study in QO can be found in [10,15,16]. Dielectric lenses have been thoroughly studied in the literature [17], and previously studied in this research group [18].

Finally, on the receiving side a RF-DC converter will be implemented outputting the transferred power. The output power is used in a feedback channel that depends on the energy received and will help in the control of the transmitter, and this way optimizing the overall WPT efficiency.

All of these components will be explained in the following sections. Starting from an overview of the system architecture, the transmitter, the basics of quasi-optics will be explained. Afterwards, the RF-DC conversion and the feedback channel will be discussed. Experimental results have been obtained for the transmitter and phased-array antenna, while simulation results have been obtained for the antenna with the dielectric lens.

2. System Architecture

The proposed system is composed of a DC-RF converter and power transmitter that will feed a phased array antenna. The beam created will be focused by a dielectric lens. Afterwards, a receiving antenna will be connected to a RF-DC converter, from which the output DC power will be obtained. A feedback channel will be implemented in order to control the transmitter output for increasing the overall efficiency. An overview of the system is represented in Fig. 1.

2.1. Active Phased Array Transmitter

The proposed Active Phased Array Transmitter consists of 16 active and independent channels that will feed a 4x4 microstrip patch antenna array operating at 5.8 GHz that should provide at least 25W to a maximum output power of 32W of RF power in a CW regime. In Fig. 2, is presented the block diagram of the transmitter and also the backscatter/receiving module. The backscatter is going to be used for feedback purposes to improve the system efficiency. Moreover, in Fig. 3, is depicted a photograph of the complete system assembled with several components, such as DC power supplies, control signals, power distribution, and fans for thermal compensation.

This system considered a LO frequency fixed at 5.1 GHz and an IF frequency of 0.7 GHz that is up-converted by a mixer to the operating frequency of 5.8 GHz. This choice is justified since a phased array must have complete flexibility to control each element's amplitude and phase difference. There are several ways to achieve this kind of operation,

reported in the literature, such as using varactors [19], time delay [20] or based on vector modulators (IQ modulators) [21]. Due to its operation simplicity, an IQ modulator is used on every element to allow the control of phase shift and/or amplitude. Each IQ modulator receives and modulates the 0.7 GHz IF signal that was previously divided into 16 equal signals, as well as the LO signal.

To implement and perform beamforming architectures, following the antenna array theory [14], the phase difference required at each element of the antenna to point the beam to a certain direction (θ_p, φ_p) , for a planar and uniform distribution is given by:

$$\psi(n, m) = k d n \sin(\theta_p) \cos(\varphi_p) + k d n \sin(\theta_p) \sin(\varphi_p), n = 1, \dots, N, m = 1, \dots, M \quad (1)$$

where k is the wavenumber, d is the inter-element spacing, and n and m are the indexes of the (n, m) element. Then to set the appropriate phase and amplitude for all 16 elements, a dense digital-to-analog converter (DAC) was selected. The chip is a complete single-supply, with 40-channel and 14-bit resolution that is controlled with the FPGA using SPI connection. With this, each DAC is controlled by a 14-bit word that will produce a signal with a certain amplitude and phase shift (ψ) , the IQ values sent to each channel in decimal representation are given by:

$$I(n, m) = \text{round}\left(\frac{2^{14}}{2} + a_{n,m} \frac{2^{14}}{2} \cos(\psi)\right) \quad (2)$$

$$I(n, m) = \text{round}\left(\frac{2^{14}}{2} + a_{n,m} \frac{2^{14}}{2} \sin(\psi)\right) \quad (3)$$

where $a_{n,m}$ is referring to the amplitude control of the (n, m) element.

Since each RF path (each channel) will present different responses in terms of phase and gain/attenuation that feeds each antenna element, a calibration procedure is needed to compensate for those differences. For that, a full calibration is needed to create a LUT that will be used to calculate the correct value to produce a radiation pattern in a specific direction in both azimuth and elevation planes.

2.2. Quasioptics for Enhancing the Beam Efficiency

One of the main losses in WPT systems are related to the beam propagation, mostly due to spillover losses and unoptimized coupling to the radiating components, resulting in low beam efficiency. Quasioptics (QO) can be used to deal with these issues since it helps understand and control microwave beams and their propagation by adapting the tools of optics to contexts with high divergence.

The fundamental block of this theory is the comparison of microwave radiation to gaussian beams: assuming a propagation in the \hat{z} direction, z_0 is the point at which the power is most concentrated and the divergence less evident. The electric field of a gaussian beam that propagates freely in the fundamental mode is axially symmetric, depending only on the distance from the axis of propagation (radius), r , and the position along the axis, z :

$$E(r, z) = \sqrt{\frac{2}{\pi\omega^2}} \exp\left(-\frac{r^2}{\omega^2} - ikz - \frac{i\pi r^2}{\lambda R} + i\phi_0\right), \quad (4)$$

where ω is the beam radius, R is the radius of curvature of the wave front, ϕ_0 is the phase shift and λ is the wavelength.

The beam radius is one of the most relevant quantities for WPT, as it is the radial distance at which the power density falls to $1/e$ of the on-axis value, with e being the Euler's number. Its minimum value is a characteristic of the beam, called the beam waist, ω_0 , located in z_0 .

Gaussian beams can be transformed using the matricial formalism: by representing any QO system through a matrix, M_{sys} ,

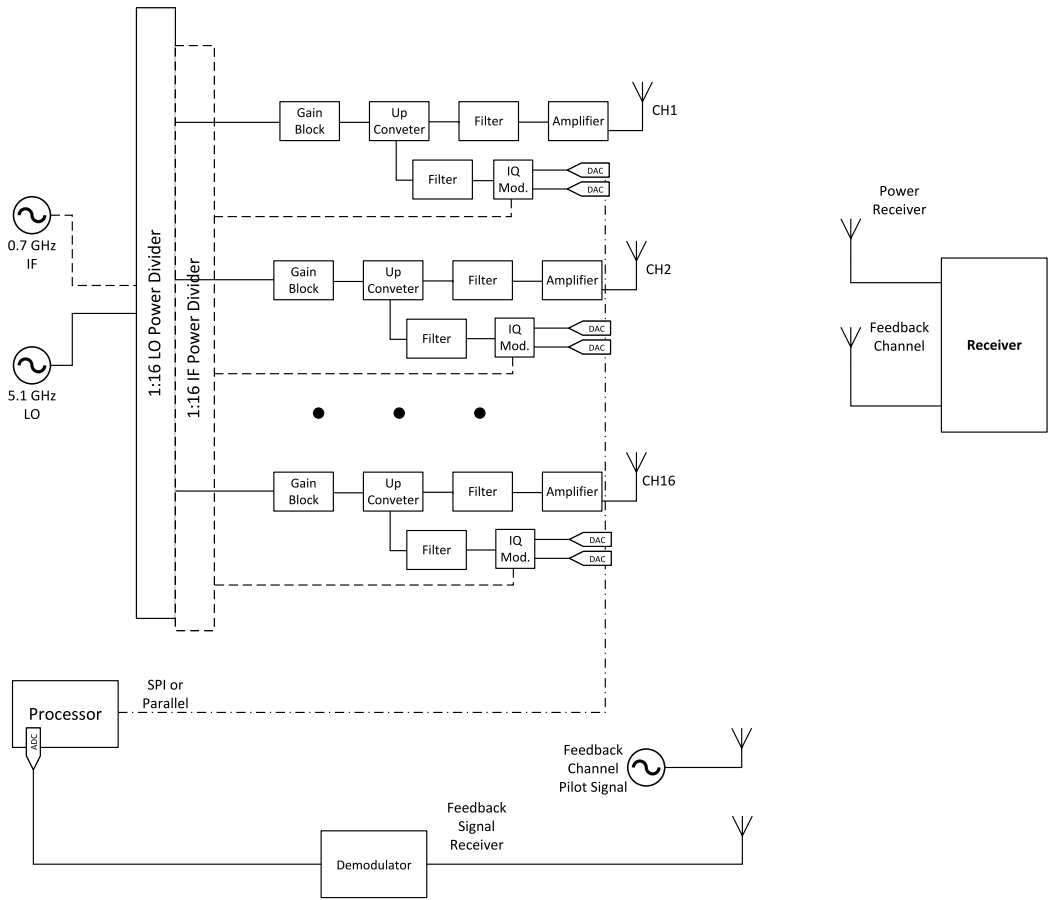


Figure 2. Block Diagram of High-Power Wireless Power Transmitter.

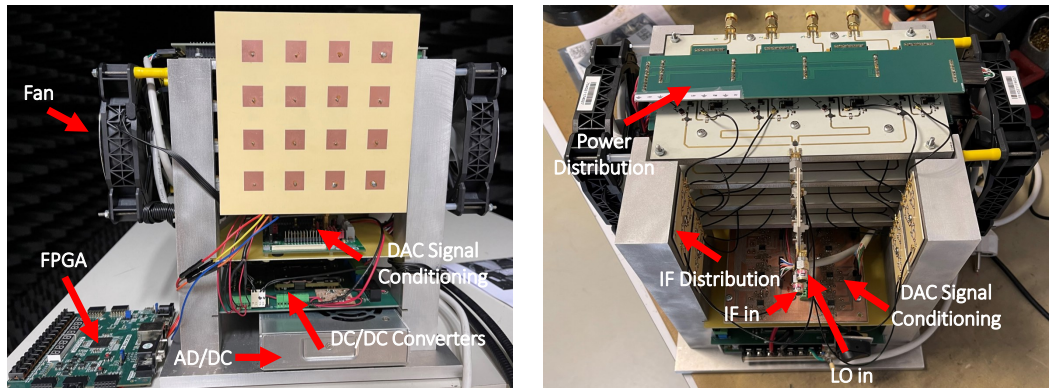


Figure 3. Full Transmitter Assembled with the several components.

$$M_{sys} = \begin{bmatrix} 1 & d_{out} \\ 0 & 1 \end{bmatrix} \cdot \begin{bmatrix} A & B \\ C & D \end{bmatrix} \cdot \begin{bmatrix} 1 & d_{in} \\ 0 & 1 \end{bmatrix} \quad (5)$$

its effect on the microwave beam can be understood by the relationship between the input and output beam waist and distance to the system, $\omega_{0_{in}}$, d_{in} and $\omega_{0_{out}}$, d_{out} , respectively:

$$d_{out} = -\frac{(Ad_{in} + B)(Cd_{in} + D) + ACz_c^2}{(Cd_{in} + D)^2 + C^2z_c^2} \quad (6)$$

and

$$\omega_{0_{out}} = \frac{\omega_{0_{in}}}{\sqrt{(Cd_{in} + D)^2 + C^2z_c^2}}. \quad (7)$$

In (7), $z_c = \pi\omega_0^2/\lambda$ is the confocal distance, a parameter which details the distance from z_0 where the beam remains collimated, presenting minimum divergence.

Finally, the coupling of gaussian beams and radiating antennas is given by a comparison between both their electric field distributions. The resulting coupling efficiency, η_G , provides information about how well the antenna radiates and receives the radiation [10,22]:

$$\eta_G = \frac{\iint |E_A \cdot E_G^*|^2 dx dy}{\left[\iint |E_A|^2 dx dy \right] \left[\iint |E_G|^2 dx dy \right]} \quad (8)$$

2.3. Antenna Array and Dielectric Lens

When attempting to transfer power, the beam efficiency must be maximized, which is done here by focusing the energy through a dielectric lens, which means the system works in the antennas' Fresnel zone. A phased array antenna composed of 4x4 microstrip patches was developed to perform beamforming and beamsteering, by controlling the current distribution of each element. These were respectively implemented according to the principles found in [13] and [14].

Knowing the expected gaussian beam radiated by the phased array, a dielectric lens was studied for transforming the beam in order to reduce the spillover losses. By keeping the beam radius smaller than the receiving aperture, the receiver collects the majority of the energy, and if it is located at the beam waist, the wave front is planar, enabling the best coupling to planar rectennas. The lens was chosen to have a spherical and elliptical surface, respectively, in order to reduce its reflectivity, and was designed according to [10,23].

2.4. Feedback Channel

In this section, we show the design and theory of the receiving node that should be able to be selected and tracked by the developed transmitter. It is used separate link for the pilot signal, the node will be able to continuously receive the energy that is being transmitted to it, while being able to scatter the pilot signal back to the transmitter with useful information. The block diagram of this node is depicted in 4. The main blocks of the receiving node are a high-power and efficient RF-to-dc converter circuit, a low-order backscatter module, an activating circuit, and a load. The remaining of this section is dedicated to provide a detailed description of each of these components.

2.4.1. RF-DC Converter

An RF-DC converter can be divided into three parts, the matching impedance network, the rectifier and the DC filter, as seen in Fig. 5a. In the case of this work, the rectifier used was a voltage multiplier.

In order to design the matching impedance network and the DC filter, it is essential to take into account the impedance that they will impose in the rectifier, as it has a significant impact on the diode's performance. So, to ensure that the blocks are matched to the rectifier,

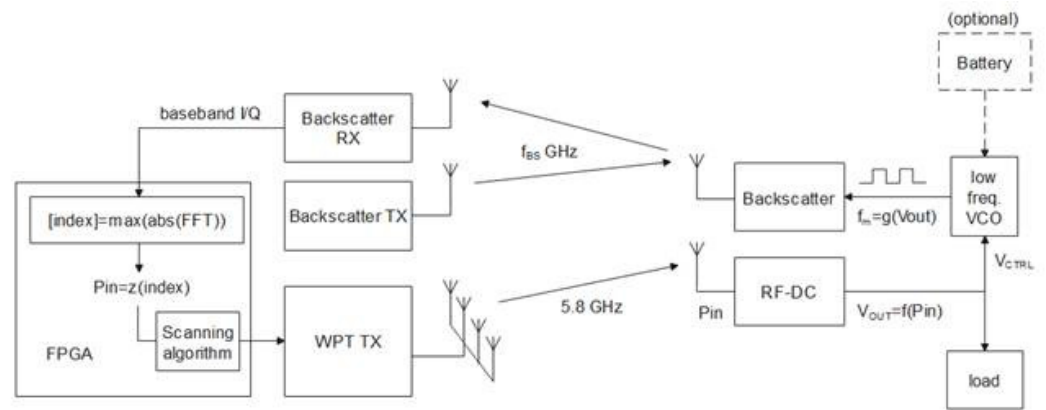


Figure 4. Feedback Channel Block Diagram.

one of the most important steps when designing an RF-DC converter is the source and load-pull simulations. For this, the ADS software was used. The schematic used for this simulation can be found in Fig. 5b. To simulate the matching impedance network, it was used the S2P_Eqn block in which the impedance Γ_{source} was made varied to find the adequate impedance for the rectifier.

On the other hand, to simulate the DC filter, the chosen block was the S1P_Eqn, in which the Γ_{load} variable was made vary to simulate the load impedance. With this simulation, it was possible to conclude that for an high input power of 30 dBm, the rectifier requires low impedance from the source's side, as it is possible to observe in Fig. 5c. In the case of the load impedance, the load-pull simulation showed that it was required an impedance of $0.064 - j0.465$.

The chosen filter for the output was a class-R filter (Fig. 5d), based on [24]. The substrate used to simulate the microstrip lines is the Rogers RO4003C with a thickness of 0.508 mm, a dielectric constant of 3.38 and a dissipation factor of 0.0027. The source-pull simulation was re-made with the R-filter implemented instead of a load block.

The final RF-DC converter can be found in Fig. 5f. The simulated efficiency results can be observed in Fig. 5g with an efficiency of 61 % for 30 dBm calculated with equation 9.

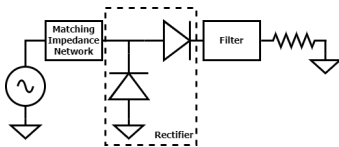
$$\eta(\%) = 100 * \frac{P_{out}}{P_{in}} = 100 * \frac{V_{out,DC}^2}{R_{out} * P_{in}} \quad (9)$$

2.4.2. Backscatter Modulator with Ring Oscillator

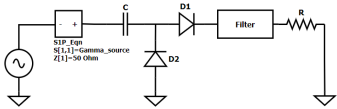
The backscattering module was based on the previous work by the group [26,27]. This is the component that allows the receiver to resend a pilot signal to the transmitter with useful information modulated in frequency, which is related to the instantaneous RF input power. To achieve this, a ring oscillator operates as a VCO in the subthreshold region, and its oscillation frequency, f_m , is shown to be dependent on the node's instantaneous RF input power. This behavior can be achieved by connecting the inverters' power rails directly to the output of the RF-to-DC converter. The relation can be understood in two steps. First, the PCE achieved by an RF-to-DC converter is a function of the input power and load. It may be measured and given by

$$PCE = \frac{P_{out,DC}}{P_{in,RF}} = \frac{V_{out,DC}^2}{R_L * P_{in,RF}}, \quad (10)$$

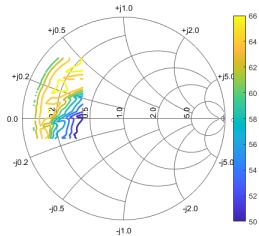
where $V_{out,DC}$ is the output DC voltage, $P_{out,DC}$ is the output DC power, $P_{in,RF}$ is the instantaneous RF input power, and R_L is the load presented to the RF-to-dc converter circuit. Thus, by characterizing the node's PCE, (10), the DC voltage produced is shown



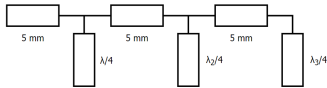
(a) RF-DC converter block diagram.



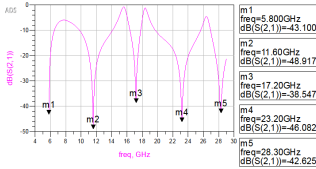
(b) Schematic of the source and load pull simulation used in ADS.



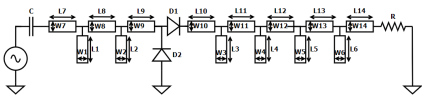
(c) Source-pull simulation.



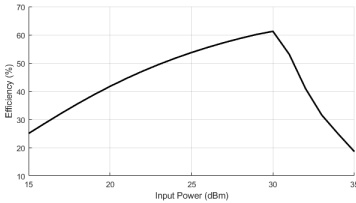
(d) Class-R filter Block Diagram.



(e) Class-R filter for a fundamental frequency of 5.8 GHz.

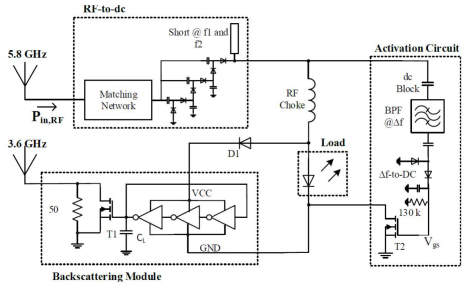


(f) Schematic of the RF-DC converter.

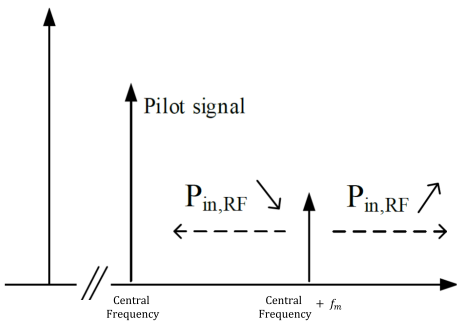


(g) Simulated efficiency.

Figure 5. High Power and Efficient RF-DC Converter Step-by-Step Design.



(a) Receiver schematic where the RF-DC converter, the bascattering module, activation circuit and a load are highlighted.



(b) Illustration of the spectrum produced by the bascattering module.

Figure 6. Backscattering module schematic and spectrum illustration. Original source [25]

to be variable and dependent on the instantaneous RF input power and load as in the following equation:

$$V_{out,DC} = \sqrt{PCE(P_{in,RF}, RL) \cdot RL \cdot P_{in,RF}}. \quad (11)$$

Secondly, if the inverters are operated in the subthreshold region, there is a strong relationship between the output current and the provided supply voltage. The capacitance C_L shown in 6a is not a real capacitor and only represents the parasitic capacitance that must be charged/discharged to switch the output of the inverter. Since the power rails are directly connected to the output of the RF-to-DC converter, the delay introduced due to the charge/discharge of C_L will be a function of $V_{out,DC}$ and will define the oscillation frequency. Since $V_{out,DC}$ is a function of the input power and load, the total delay, d , can be represented as follows (assuming a constant R_L):

$$d = g(P_{in,RF}) \quad (12)$$

and the oscillation frequency produced by the ring oscillator is given by

$$f_m = \frac{1}{2d} = \frac{1}{2g(P_{in,RF})} \quad (13)$$

where g is the relationship between the total delay and the RF input power ($P_{in,RF}$). Note that g can also be obtained from measurements. This modulation frequency will be used to drive the backscatter modulator. A spectral representation of what is the goal is depicted in Fig. 6b. By knowing the g function, the backscattered pilot signal can be decoded in real time and an accurate estimation of the node's available RF input power can be taken by inverting (13). This way, the nodes can also be considered as real-time passive wireless power probes. Since WSN nodes are devices that usually do not need to transmit more than a few bytes of information, the backscattered signal can be further modulated by an alternative modulation, e.g., amplitude modulation, with the sensor/device information at a low transmission rate. This can be implemented with a low-power AND gate, for example.

3. Preliminary Results and Discussion

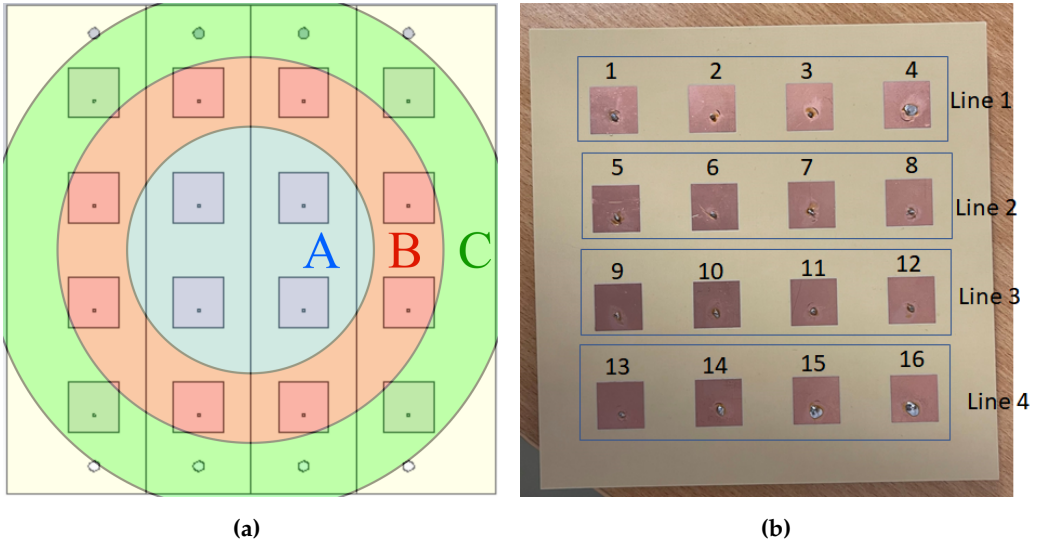
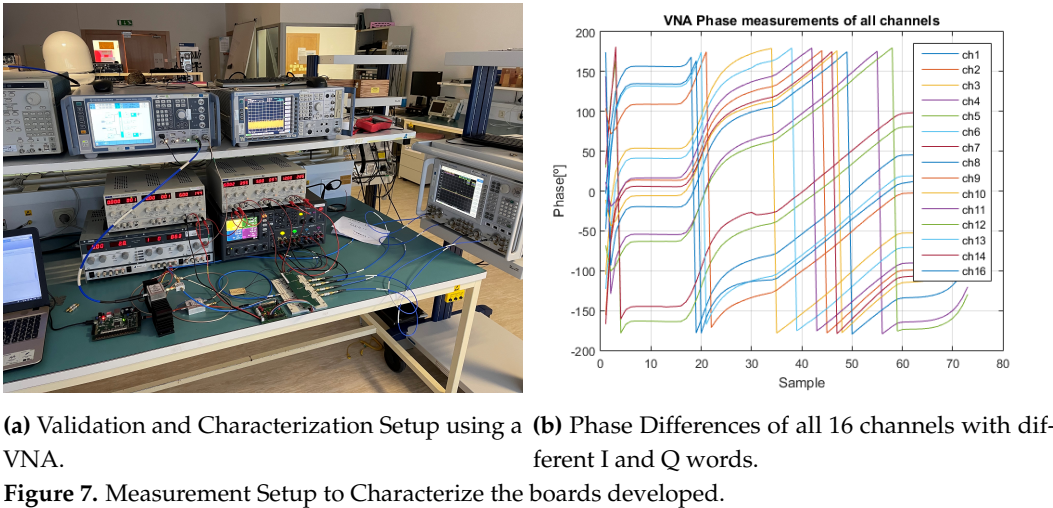
This section is presented several results, both measured and simulated, obtained until the moment for the different parts of the system. Further analysis will be performed in each of the following subsections.

3.1. RF Boards Validation

With the first characterization setup was intended to characterize each one of the four boards developed, in terms of the amplitude and phase of the output signal. For a setup composed by a VSG that is responsible for generate the LO and IF frequencies (5.1 GHz and 700 MHz respectively), power supply sources that provide the DC bias for the different elements in the boards. Then each output of the board is connected to a VNA that will measure the amplitude and phase of the received signals, as shown in Fig. 7.

In Fig.7 is presented the phase of all of 16 channels. It is possible that with the several combinations of I and Q words is possible to cover a frequency range of 360° (from -180° to 180°). The amplitude of each channel is not presented since for this characterization the amplitude was maintained equal to 1.

With the values obtained is intended to create a LUT in order to be able, in the future, to control in real time the phase of each channel and provide beamforming capabilities to the system.



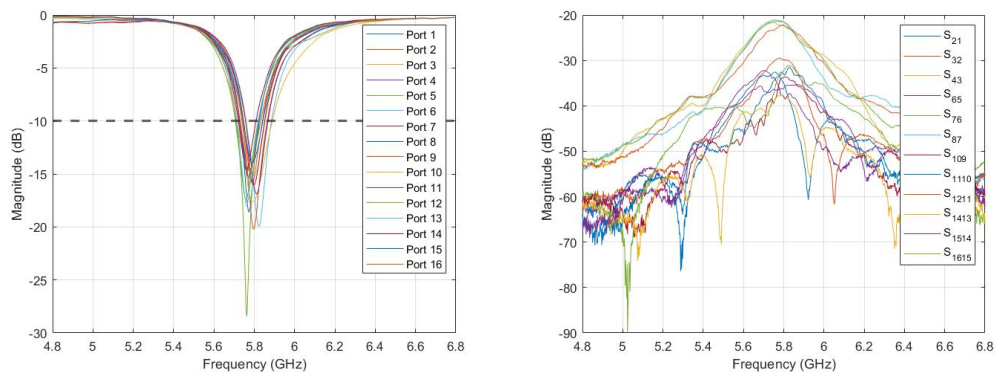
3.2. Microwave Beam Focusing

The energy focus is created by generating a gaussian beam with a phased array and later transforming it through a dielectric lens.

3.2.1. Microstrip Patch Phased-Array Antenna

As described previously, the gaussian beam launcher is a phased array that was designed, simulated and optimized for the frequency of operation of 5.8 GHz in CST Studio Suite, before being built. This optimization resulted in a 4x4 array, composed of identical square patches. These are fed by a coaxial connector on the ground plane, located slightly below the patches' center. The optimized antenna in CST is visible in Fig. 8a next to the final manufactured array in Fig. 8.

Using this antenna, a study was performed for understanding how to generate different gaussian beams, according to the project's needs. The beamforming was achieved by altering each elements' current distribution [13], whose results are described in Table 2. The Firstly, the elements were separated in groups, according to their distance from the antenna's central point. This resulted in three groups, described in Table 1.



(a) Return loss of each element. (b) Coupling between elements of the same row.

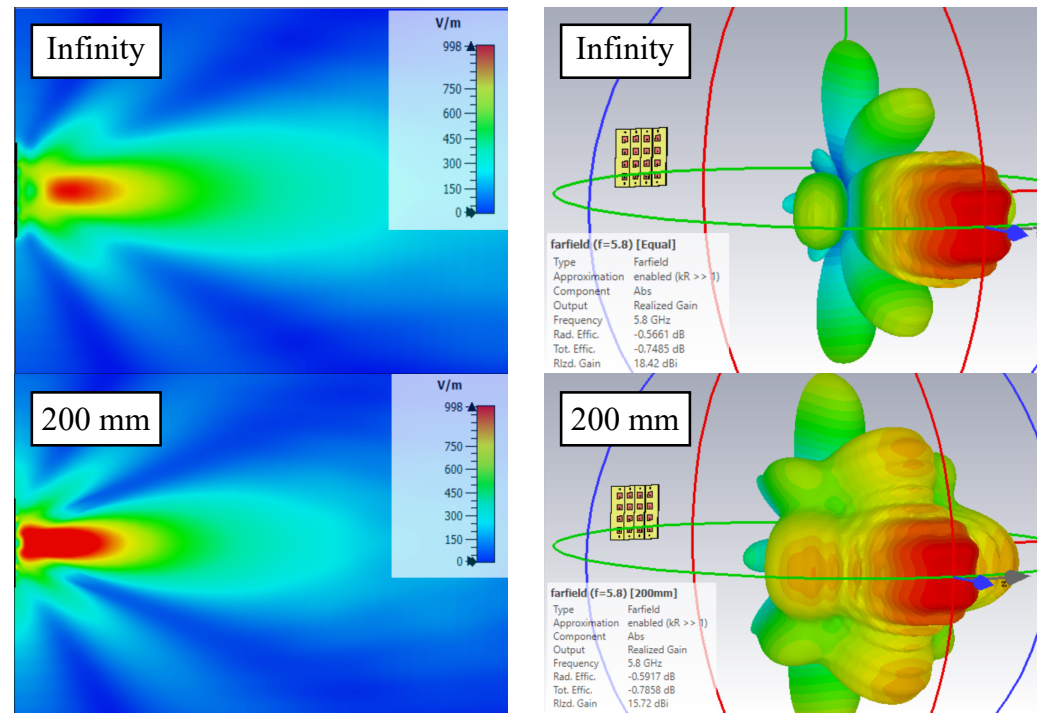
Figure 9. Experimental results of the phased array designed for wireless power transfer containing the return loss of each element (a) and the coupling between elements of the same row (b).

Table 1. Phased-array element separation into groups, according to the distance from each patch center to the overall array central point, where w is the *patch width* and d is the *element separation*.

Group	Distance	Value [mm]	Elements
A	$(d + w) / \sqrt{2}$	94.165	6, 7, 10, 11
B	$(d + w) \sqrt{5/2}$	70.187	2, 3, 5, 8, 9, 12, 14, 15
C	$3(d + w) / \sqrt{2}$	31.388	1, 4, 13, 16

Table 2. Details of the radiation produced by varying the electric current distribution feeding the phased array.

Beam waist location	Max. E_{field} [V/m]	Max. E_{field} location [mm]	Gain [%]	Efficiency [%]
Infinity	998.261	92.343	18.42	84.17
1000 mm	1153.88	77.586	18.34	84.16
500 mm	1302.12	72.220	18.02	84.08
400 mm	1369.59	69.537	17.77	84.01
300 mm	1471.02	64.171	17.23	83.97
200 mm	1635.17	53.439	15.72	83.45



(a) Electric field distribution.

(b) Radiation pattern.

Figure 10. Comparison of the phased array antenna's electric field distribution (a) and far field gain (b), for a focus at infinity and at 200 mm from the antenna. The results are summarized in Table 2.

The electric field distribution and antenna gains of the most extreme cases, for a focus at infinity and a focus location at 200 mm, are represented in Fig. 10.

Following this study, the antenna array was printed in a PCB and the connectors were soldered to each element's back. This enabled the measurement of each elements' return loss and coupling to elements in the same line (Fig. 8b), as depicted in Fig. 8. All the elements present a return loss of under -10 dB for 5.8 GHz, and coupling between elements of the same line is under -20 dB, both being acceptable values.

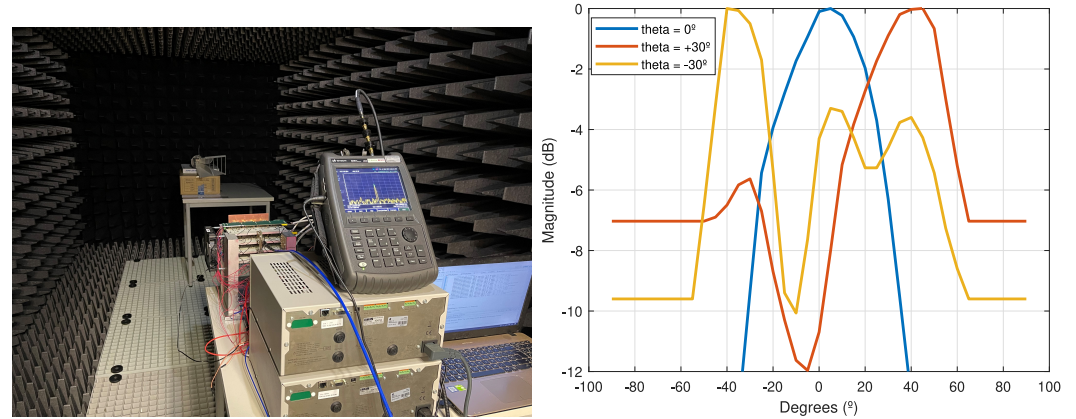
The array was then connected to the transmitter board described previously and the complete transmitting system was analyzed in an anechoic chamber, with beam steering having been performed.

3.2.2. Transmitter Radiation Pattern

After validating each PCB and hardware in a laboratory environment, the system was taken to the anechoic chamber in order to measure the radiation pattern, using the results obtained in 3.1. As shown in Fig. 11, the measurement setup was mounted on the anechoic chamber with the goal of measuring the radiation pattern in several azimuth angles (0° , $+30^\circ$, and -30°). For that, the transmitter was rotated manually from -45° to 45° with a step of 5° . The results of these measurements are presented in Fig. 11b, and it is possible to observe that, although there is no calibration whatsoever, the results obtained are close to what was expected. With the feedback channel and intelligent algorithms to calculate the necessary amplitudes and phases, the beamwidth will be narrower and provide higher gain and efficiency than what was presented here.

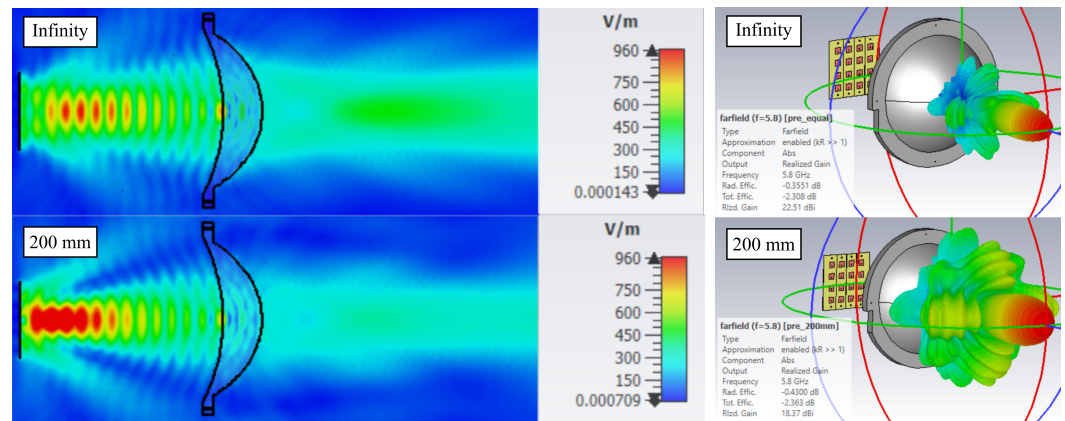
3.2.3. Dielectric Lens

Having studied the phased array, its radiation will be focused by a dielectric lens, in order to create focus of energy. The lens' design that was chosen has a spherical and elliptical surface, respectively, for reducing its reflection. The design was based on the principles found in [23].



(a) Measurement Setup in Anechoic Chamber. (b) Radiation pattern.

Figure 11. Transmitter Radiation Pattern for different Azimuth Angles and respective Measurement Setup.



(a) Electric field of the antenna and lens.

(b) Gain of the antenna and lens.

Figure 12. Comparison of the phased array antenna and lens' electric field distribution (a) and far field gain (b), for a focus at infinity and located at 200 mm from the antenna.

The antenna and lens system was also simulated in CST. This complete transmission system has the electric field distribution and far field represented in Fig. 12. The results obtained are summarized in Table 3.

One can conclude that the beam focused by the dielectric lens is more directive, which is necessary for high efficiency wireless power transfer. However, the analysis of the gaussian beam still needs to be further developed as the beam outputted from the phased array needs to be determined.

4. Conclusions

This work reports a high-power and efficient Wireless Power Transmitter for charging mobile devices. The proposed system is composed of 16 independent channels that can provide up to 2W and control over the amplitude and phase of each channel, forming a high-power active phased array for WPT purposes. Then, since most of the energy is typically lost in the beam propagation due to free space losses, an innovative approach based on QO theory is proposed for enhancing the beam efficiency and, consequently, the overall system efficiency. To do that, a dielectric lens will create a focus of energy in the Fresnel zone, significantly reducing the spillover losses.

On the receiving side (mobile device), a feedback channel is implemented that allows the transmitter to locate the received node and improve power transmission efficiency. The receiving node is composed of an RF-DC converter that will convert the RF energy into electrical power. This electrical power will supply a low-frequency oscillator and a

Table 3. Far-field simulation results of just the phased-array (T_x) and phased-array and lens radiating system ($T_x + \text{Lens}$).

Beam waist location	Gain [dBi]		Efficiency [%]	
	T_x	$T_x + \text{Lens}$	T_x	$T_x + \text{Lens}$
Infinity	18.42	24.25	84.17	84.62
1000 mm	18.34	23.92	84.16	84.51
500 mm	18.02	23.36	84.08	84.09
400 mm	17.77	22.99	84.01	83.78
300 mm	17.23	22.25	83.87	83.12
200 mm	15.72	20.35	83.45	81.52

backscatter modulator that will transmit a signal back to the transmitter, which frequency will depend on the power received by the RF-DC converter. This way is possible to know how far the receiving node is. Finally, some preliminary results (measured and simulated) are presented regarding the several parts of the system that show a very good initial results that prove the feasibility of the system for indoor environment mobile devices charging. Therefore, with the implementation of machine learning or artificial intelligence algorithms on the transmitter will allow to have commercial WPT systems for device charging.

Author Contributions: All the authors have contributed to this paper. Diogo Matos has designed all the transmitter hardware, performed the characterization of the transmitter and wrote the paper. Ricardo Pereira has developed the quasioptics theory for WPT, has designed and simulated the antenna and dielectric lens and wrote the paper. Helena Ribeiro has designed the RF-DC converter and wrote the paper. Bernardo Mendes has been responsible for the digital control and the characterization of the transmitter. Arnaldo Oliveira has supervised the entire research with more focus in digital component, the results analysis and discussion and provided the guidance for writing the paper. Nuno Borges Carvalho has supervised the entire research in RF component, the used approach, the results analysis and discussion and provided the guidance for writing the paper. All authors have read and agreed to the published version of the manuscript.

Acknowledgments: The authors would like to thank to Huawei Sweden for the support and collaboration in this work. On the other hand, Ricardo Pereira would like to thank the Fundação para a Ciência e a Tecnologia (FCT), Portugal for his Ph.D. grant SFRH/BD/145024/2019.

Conflicts of Interest: The authors declare no conflict of interest.

Abbreviations

The following abbreviations are used in this manuscript:

CW	Continuous-Wave
DAC	Digital-to-Analog Converter
DC-RF	Direct Current to Radio Frequency
EM	Electromagnetic
FPGA	Field Programmable Gate Array
IF	Intermediate Frequency
IQ	In-phase and quadrature
LO	Local Oscillator
LUT	LookUp Table
PCE	Power Conversion Efficiency
PCB	Printed Circuit Board
QO	Quasioptical
RF	Radio Frequency
RF-DC	Radio Frequency to Direct Current
SPI	Serial Peripheral Interface
VCO	Voltage Controlled Oscillator
VNA	Vector Network Analyzer
VSG	Vector Signal Generator
WPT	Wireless Power Transmission

References

1. Brown, W.C. The History of Power Transmission by Radio Waves. *IEEE Transactions on Microwave Theory and Techniques* **1984**, 32, 1230–1242. doi:10.1109/TMTT.1984.1132833.

2. Marincic, A.S. Nikola Tesla and the Wireless Transmission of Energy. *IEEE Transactions on Power Apparatus and Systems* **1982**, PAS-101, 4064–4068. doi:10.1109/TPAS.1982.317084.

3. Lumpkins, W. Nikola Tesla’s Dream Realized: Wireless power energy harvesting. *IEEE Consumer Electronics Magazine* **2014**, 3, 39–42. doi:10.1109/MCE.2013.2284940.

4. Jawad, A.M.; Nordin, R.; Gharghan, S.K.; Jawad, H.M.; Ismail, M. Opportunities and Challenges for Near-Field Wireless Power Transfer: A Review. *Energies* **2017**, 10. doi:10.3390/en10071022.

5. Kim, H.J.; Hirayama, H.; Kim, S.; Han, K.J.; Zhang, R.; Choi, J.W. Review of Near-Field Wireless Power and Communication for Biomedical Applications. *IEEE Access* **2017**, 5, 21264–21285. doi:10.1109/ACCESS.2017.2757267.

6. Brown, W.C. The history of wireless power transmission. *Solar Energy* **1996**, 56, 3–21. Wireless Power Transmission, doi:https://doi.org/10.1016/0038-092X(95)00080-B.

7. Shinohara, N. History of Research and Development of Beam Wireless Power Transfer. 2018 IEEE Wireless Power Transfer Conference (WPTC), 2018, pp. 1–4. doi:10.1109/WPT.2018.8639249.

8. Shinohara, N. History and Innovation of Wireless Power Transfer via Microwaves. *IEEE Journal of Microwaves* **2021**, 1, 218–228. doi:10.1109/JMW.2020.3030896.

9. Rodenbeck, C.T.; Jaffe, P.I.; Strassner II, B.H.; Hausgen, P.E.; McSpadden, J.O.; Kazemi, H.; Shinohara, N.; Tierney, B.B.; DePuma, C.B.; Self, A.P. Microwave and Millimeter Wave Power Beaming. *IEEE Journal of Microwaves* **2021**, 1, 229–259. doi:10.1109/JMW.2020.3033992.

10. Goldsmith, P.F. *Quasioptical Systems: Gaussian Beam Quasioptical Propagation and Applications*; IEEE Press: Piscataway, NJ,, 1998.

11. Pereira, R.A.M.; Carvalho, N.B.; da Cunha, J.P. Quasi-optical analysis of a double reflector microwave antenna system. *Wireless Power Transfer* **2018**, 5, 75–86. doi:10.1017/wpt.2017.19.

12. Pereira, R.A.M.; Carvalho, N.B.; Georgiadis, A. Focus Location Measurement of a Quasioptical Double Reflector System. 2021 IEEE Wireless Power Transfer Conference (WPTC), 2021, pp. 1–4. doi:10.1109/WPTC51349.2021.9457870.

13. Takano, T.; Uno, T.; Shibata, K.; Saegusa, K. Generation of a beamed wave using a phased array antenna. 2016 URSI Asia-Pacific Radio Science Conference (URSI AP-RASC), 2016, pp. 377–379. doi:10.1109/URSIAP-RASC.2016.7601247.

14. Balanis, C.A. *Antenna Theory: Analysis and Design*; John Wiley & Sons, Inc.: Hoboken, NJ, 2005.

15. Kim, W.G.; Moon, N.W.; Singh, M.K.; Kim, H.K.; Kim, Y.H. Characteristic analysis of aspheric quasi-optical lens antenna in millimeter-wave radiometer imaging system. *Appl. Opt.* **2013**, 52, 1122–1131. doi:10.1364/AO.52.001122.

16. Qin, Y.; Guo, Q. Quasi optic lens antenna with corrugated feed horns. ICMMT’98. 1998 International Conference on Microwave and Millimeter Wave Technology. Proceedings (Cat. No.98EX106), 1998, pp. 382–386. doi:10.1109/ICMMT.1998.768306.

17. Fernandes, C.A.; Costa, J.R.; Lima, E.B.; Silveirinha, M.G. Review of 20 Years of Research on Microwave and Millimeter-wave Lenses at "Instituto de Telecomunicaço~es". *IEEE Antennas and Propagation Magazine* **2015**, 57, 249–268. doi:10.1109/MAP.2015.2397156.

18. Gonçalves, R.; Carvalho, N.B.; Pinho, P. Wireless energy transfer: Dielectric lens antennas for beam shaping in wireless power-transfer applications. *Comptes Rendus Physique* **2017**, 18, 78–85. Energy and radiosciences, doi:10.1016/j.crhy.2016.11.004.

19. Zhang, H.; Ren, H.; Tang, H.; Zheng, B.; Katz, B.; Arigong, B.; Zhang, H. A Microstrip line Reflection-Type Phase Shifter for 60 GHz Phased Array. 2019 IEEE MTT-S International Microwave Symposium (IMS), 2019, pp. 826–829. doi:10.1109/MWSYM.2019.8700849.

-
20. Masotti, D.; Costanzo, A.; Del Prete, M.; Rizzoli, V. Time-Modulation of Linear Arrays for Real-Time Reconfigurable Wireless Power Transmission. *IEEE Transactions on Microwave Theory and Techniques* **2016**, *64*, 331–342. doi:10.1109/TMTT.2015.2512275.
 21. Yang, W.; Zhou, J.; Zhou, K.; Yu, Z. A 5.8-GHz Active Transmitting Array Based on Frequency Shiftable Vector Modulator Module. *IEEE Antennas and Wireless Propagation Letters* **2016**, *15*, 1085–1088. doi:10.1109/LAWP.2015.2493200.
 22. Karandikar, Y. Factorization of Gaussian Coupling Efficiency and algorithm to compute it. 2012 6th European Conference on Antennas and Propagation (EUCAP), 2012, pp. 868–872. doi:10.1109/EuCAP.2012.6205837.
 23. Lo, Y.T.; Lee, S.W. *Antenna Handbook: Volume II Antenna Theory*; Van Nostrand Reinhold: New York, NY, 1993.
 24. Miwatashi, K.; Shinohara, N. Development of Class-R Rectifier for Microwave Wireless Power Transmission to EV trucks. 2021 IEEE Wireless Power Transfer Conference (WPTC), 2021, pp. 1–4. doi:10.1109/WPTC51349.2021.9457968.
 25. Belo, D.; Ribeiro, D.C.; Pinho, P.; Carvalho, N.B. A Low Complexity and Accurate Battery-Less Trackable Device. 2018 IEEE/MTT-S International Microwave Symposium - IMS, 2018, pp. 1269–1271. doi:10.1109/MWSYM.2018.8439502.
 26. Correia, R.; Boaventura, A.; Borges Carvalho, N. Quadrature Amplitude Backscatter Modulator for Passive Wireless Sensors in IoT Applications. *IEEE Transactions on Microwave Theory and Techniques* **2017**, *65*, 1103–1110. doi:10.1109/TMTT.2017.2661262.
 27. Belo, D.; Ribeiro, D.C.; Pinho, P.; Borges Carvalho, N. A Selective, Tracking, and Power Adaptive Far-Field Wireless Power Transfer System. *IEEE Transactions on Microwave Theory and Techniques* **2019**, *67*, 3856–3866. doi:10.1109/TMTT.2019.2913653.